Magnetic resonance reversals in optically pumped alkali-metal vapor

F. Gong, Y.-Y. Jau, and W. Happer
Department of Physics, Princeton University, Princeton, New Jersey 08544, USA
(Received 30 January 2007; published 25 May 2007)

We report an unusual phenomenon, peculiar sign reversals of the ground-state magnetic resonances and of the zero-dip resonance (Zeeman resonance at zero field) of optically pumped, alkali-metal vapors. These anomalies occur when a weak circularly polarized $D1$ laser light is tuned to pump atoms predominantly from the lower ground-state hyperfine multiplet. One can understand the signal reversals in a simple, semiquantitative way with reference to the spin-temperature distribution. Quantitative computer simulations are in excellent agreement with observations.

DOI: 10.1103/PhysRevA.75.053415 PACS number(s): 32.80.Bx, 32.30.Dx, 32.10.Fn, 32.30.Bv

In this paper, we describe an unusual phenomenon that we have noticed for alkali-metal vapor that is optically pumped with $D1$, circularly polarized laser light. For certain optical frequencies, sufficiently weak light causes the vapor to become more opaque, while more intense light of the same frequency causes the vapor to become more transparent. This is in marked contrast to all previous observations that we know of, where pumping with circularly polarized $D1$ light increases the transparency of the vapor.

In Fig. 1 we review how circularly polarized resonance light would pump a hypothetical alkali-metal atom with no nuclear spin. Circularly polarized light "burns out" the spin-down atoms of the ground state. When the optical pumping light greatly exceeds the spin relaxation rate of ground-state atoms, nearly all the atoms will be pumped to the spin-up state. This decreases the opacity of the atoms for $D1$ light and increases the opacity for $D2$ light.

It is convenient to define a photon absorption cross section $\sigma=\sigma_{\rm op}(\nu)$ for photons of frequency ν such that the photon absorption rate per unpolarized atom is

$$\Gamma_{\rm op}=\sigma_{\rm op}\mathcal{S}/h\nu. \tag{1}$$

Here $\mathcal{S}$ is the optical energy flux (erg cm^{-2} s^{-1}). Because the optical pumping can spin-polarize the atom, the actual absorption rate $\langle\delta\Gamma\rangle$, where $\delta\Gamma$ is the photon absorption operator [1], can be larger or smaller than $\Gamma_{\rm op}$, and we write it as

$$\langle\delta\Gamma\rangle=\langle A\rangle\Gamma_{\rm op}. \tag{2}$$

The *specific absorption* $A\equiv\delta\Gamma/\Gamma_{\rm op}$ is a ground-state spin operator with an expectation value $\langle A\rangle=1$ for unpolarized atoms. If a hypothetical alkali-metal atom with no nuclear spin is pumped with σ^+ light, the specific absorption operator for $D1$ pumping light is $A=1-2S_z$, where S_z is the longitudinal electron spin operator of the ground-state atoms; for $D2$ light, $A=1+S_z$. In Fig. 1 we have assumed that the repopulation pumping comes from spontaneous decay with negligible collisional depolarization or quenching of the excited atoms. At high buffer gas pressures, where the repopulation pumping by $D2$ light is suppressed, Fricke *et al.* [2] have shown that the sign of the spin polarization reverses. We assume that diffusion to the walls and collisions with buffer gas atoms cause the longitudinal spin to relax at the rate $\langle\dot{S}_z\rangle=-\Gamma_s\langle S_z\rangle$. Then the specific absorption for $D1$ light is $\langle A\rangle=3\Gamma_s/(2\Gamma_{\rm op}+3\Gamma_s)$, while for $D2$ light we find $\langle A\rangle=(3\Gamma_{\rm op}+6\Gamma_s)/(2\Gamma_{\rm op}+6\Gamma_s)$. As indicated in Fig. 1, increasing the intensity of the circularly polarized pumping light causes the specific absorptions to approach the limits $\langle A\rangle\to 0$ for $D1$ light and $\langle A\rangle=3/2$ for $D2$ light. In both cases the limit is approached monotonically.

With this ideal behavior in mind, we turn to what is actually observed experimentally for real alkali-metal atoms with $I\neq 0$. Our apparatus is shown in Fig. 2. A Pyrex glass cell containing a small amount of Cs metal and buffer gas (50 torr N_2 and 280 torr Ar) was used. The space between the front and rear walls of the cell is $l=0.1$ cm. The cell was mounted in a temperature-controlled, air-heated nonmagnetic oven. Three sets of Helmholtz coils were used to cancel the ambient magnetic field (down to no more than 20 mG) and to produce a small longitudinal static field B, parallel to the pumping light. To drive magnetic resonances with $\Delta f=\pm 1$, microwaves from a frequency synthesizer were beamed onto the cell from a horn antenna located 10 cm away. The light from a diode laser, stabilized by an external cavity, and operating at the 895-nm Cs $D1$ line, was circularly polarized, and neutral density filters were used to control the beam intensity. The light transmitted through the optically pumped Cs cell was continuously monitored using a photodiode. The photodiode dark current was negligible. The output signal from the photodiode was amplified, digitized, and recorded. To record the hyperfine magnetic resonances, we swept B continuously from one direction to the other and recorded the transmitted light intensity. A Fabry-Pérot interferometer and a wavemeter were used to monitor the performance of the laser.

The voltage output of the photodiode of Fig. 2 is $V=V_0\exp(-[{\rm Cs}]\sigma_{\rm op}\langle A\rangle l)$ where the parameter V_0 is proportional to the laser light intensity and also includes scattering and attenuation losses of the glass walls of the oven and the glass cell. The number density of Cs atoms, [Cs], is mainly controlled by the temperature of the cell. The experimental specific absorption $\langle A\rangle$ is defined by $l\langle A\rangle=\int_0^l {\rm Tr}(\rho A)dz$, averaged along all length elements dz of the optical path through the vapor. The density operator $\rho=\rho(z)$ can vary along the optical path length through the vapor, since the light can be attenuated substantially for $[{\rm Cs}]\sigma_{\rm op}l>1$, espe-

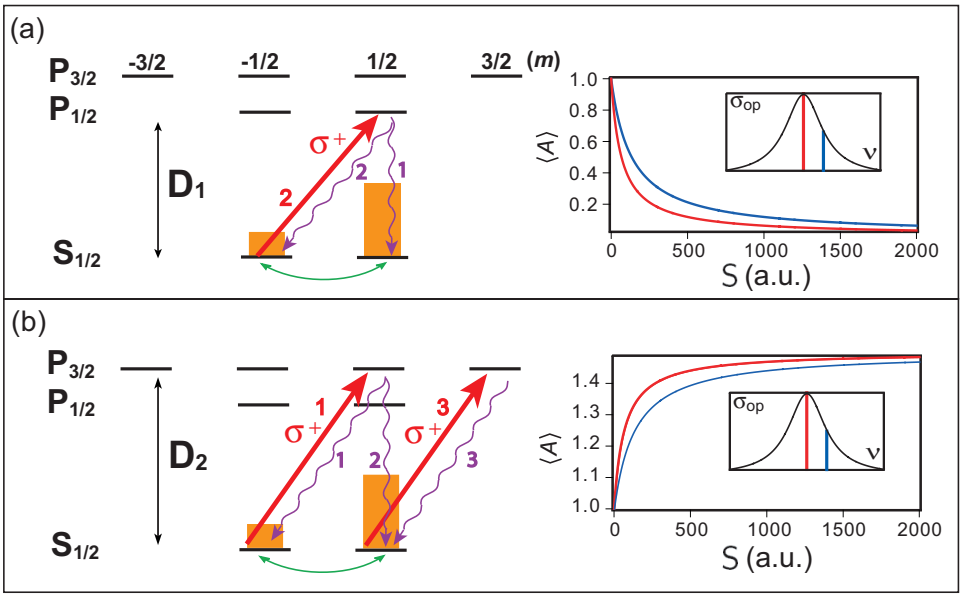

FIG. 1. (Color online) Energy sublevels of a hypothetical atom with $I=0$. Specific absorptions $\langle 1/2|A|1/2\rangle$ and $\langle -1/2|A|-1/2\rangle$ and their relative values are denoted by the diagonal arrows pointing up. Spontaneous decay and relative branching ratios are indicated by numbers on the wavy arrows pointing down. Ground-state spin relaxations are denoted by the curved double-end arrows. The bars on each ground-state sublevel are steady-state occupation probabilities for $\Gamma_{op}=\Gamma_s$. The insets show that, as the optical pumping flux $\mathcal{S}$ increases, the specific absorption $\langle A\rangle$ decreases monotonically from 1 to 0 for $D1$ pumping, and it increases monotonically from 1 to 3/2 for $D2$ pumping. Detuning the laser from the maximum of the cross section to half maximum simply stretches out the curves.

cially for low laser powers, and less so at higher powers where intense, circularly polarized light can burn through the vapor by pumping most of the atoms into the nonabsorbing end states. The specific absorption was determined from four measured photodiode voltages: (i) V_{C0}, the voltage at the photodiode produced by circularly polarized laser light at room temperature when $[\mathrm{Cs}]\sigma_{op}\langle A\rangle l \ll 1$; (ii) $V_C = V_{C0}\exp(-[\mathrm{Cs}]\sigma_{op}\langle A\rangle l)$, the voltage at the photodiode produced by circularly polarized laser light at the temperature, magnetic field, microwave power, and polarization of the experiment; (iii) V_{L0}, the voltage at the photodiode produced by linearly polarized light at room temperature when $[\mathrm{Cs}]\sigma_{op}\langle A\rangle l \ll 1$; (iv) $V_L = V_{L0}\exp(-[\mathrm{Cs}]\sigma_{op} l)$, the voltage at the photodiode produced by linearly polarized laser light at the temperature of the experiment. The experimentally determined specific absorption was then given by

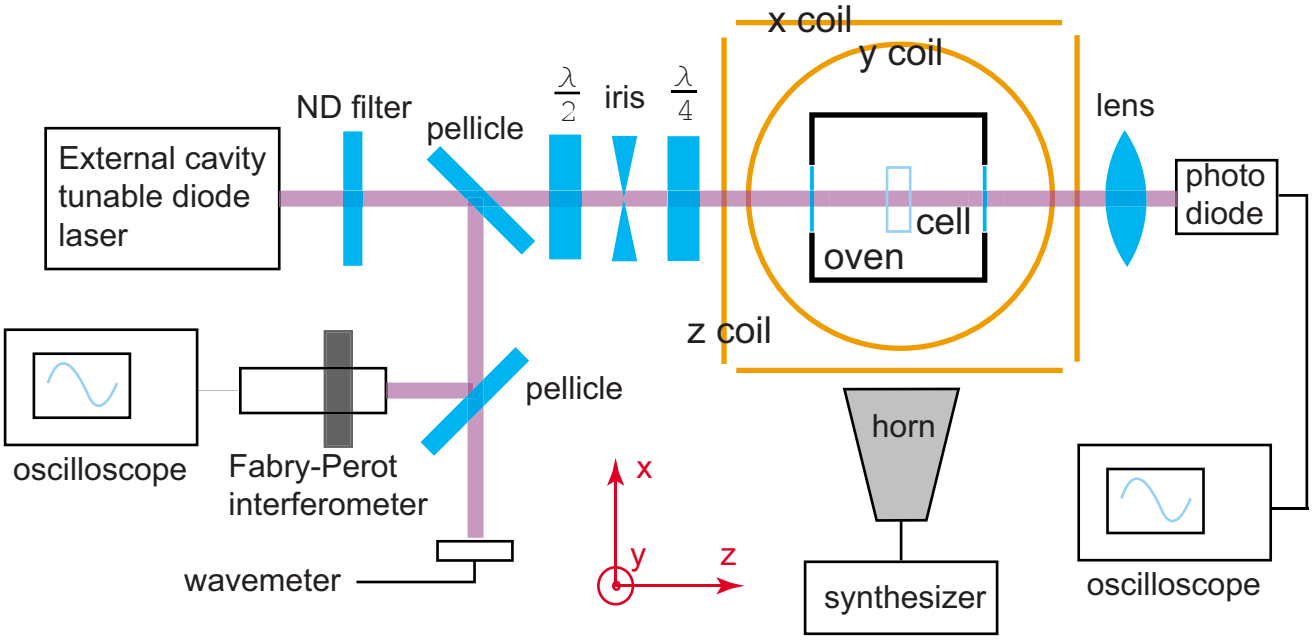

FIG. 2. (Color online) Apparatus (see text).

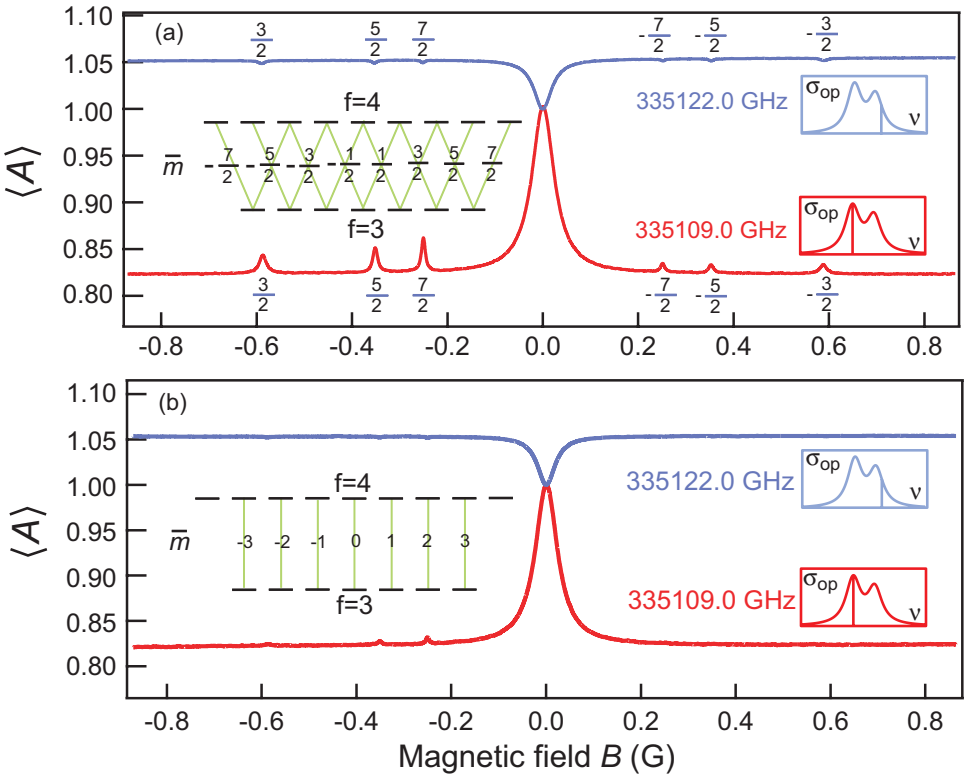

FIG. 3. (Color online) Specific absorption $\langle A\rangle$ versus longitudinal magnetic field B curves when the oscillating magnetic field is perpendicular (a) and parallel (b) to the static longitudinal field and the direction of the laser beam. Upper traces are for the laser frequency of 335 109.0 GHz. Lower traces are for 335 122.0 GHz. The two insets on the right show the cross-section curve for unpolarized atoms and the frequency positions of the two laser detunings. The insets on the left show the label $\bar{m}$ for the possible transitions that are excited by the oscillating magnetic field.

$$\langle A\rangle = \ln\left(\frac{V_C}{V_{C0}}\right) \Big/ \ln\left(\frac{V_L}{V_{L0}}\right). \tag{3}$$

The high temperatures and the resulting high spin-exchange rates efficiently destroy the hyperfine polarizations $\langle \mathbf{I}\cdot\mathbf{S}\rangle$ and birefringent polarizations $\langle 3f_z^2 - f(f+1)\rangle$ that can be produced by linearly polarized pumping light [3]. This ensured that taking $\langle A\rangle = 1$ for linearly polarized light was a good approximation. In general cases where the spin-temperature distribution is not necessarily valid, the denominator in Eq. (3) should be the value when the pumping intensity is low enough not to polarize the atoms.

Figure 3 shows the observed specific absorption $\langle A\rangle$ versus magnetic field B. Unlike the hypothetical atom with $I=0$ that was discussed in connection with Fig. 1, where $\langle A\rangle \leq 1$ for any laser detuning, the data of Fig. 3 shows that for the real Cs atom, with $I=7/2$, we observe $\langle A\rangle \leq 1$ for a laser frequency of 335 109.0 GHz (the lower trace), which pumps predominantly out of ground-state sublevels with total angular momentum quantum numbers $f=I+1/2=4$, but for small laser powers we observe $\langle A\rangle \geq 1$ for a laser frequency of 335 122.0 GHz (the upper trace), which pumps predominantly out of ground-state sublevels with total angular momentum quantum numbers $f=I-1/2=3$. At the 130 °C temperature of the cell, the unpolarized Cs vapor attenuated the 335 109.0 GHz light by 2.9 e-foldings, and it attenuated the 335 122.0 GHz light by 1.3 e-foldings. The circularly polarized incident laser power density $\mathcal{S}$ was 0.6–0.9 mW cm^{-2}. In Fig. 3(a) the magnetic field of the microwaves oscillates perpendicular to the static magnetic field and excites transitions with $\Delta m = \pm 1$ and $\Delta f = \pm 1$. In Fig. 3(b) the microwave field oscillates nearly parallel to the static magnetic field, and it can efficiently excite transitions with $\Delta m = 0$ and $\Delta f = \pm 1$. The transitions are labeled with $\bar{m}$, the average of the azimuthal quantum numbers of the initial and final states. The large resonance at zero magnetic field comes from the depolarization induced by the transverse static magnetic field, which remains when the longitudinal field passes through zero. This "zero dip" could be broader or narrower, depending on how carefully we zeroed out the transverse field.

A second interesting conclusion that can be drawn from Fig. 3 is that the two sublevels $|4m\rangle$ and $|3m\rangle$ with the same azimuthal spin quantum number m must have very nearly the same populations, since the $\Delta m = 0$ resonances are not observed. The barely visible resonances that can be seen in the lower trace of Fig. 3(b) are actually resonances with $\Delta m = \pm 1$ that result from a slight misalignment of the microwave horn and the static magnetic field. Equal populations of the sublevels $|4m\rangle$ and $|3m\rangle$ are a characteristic of the spin-temperature distribution [4] when the sublevel populations, the diagonal elements of the atomic density operator ρ, are $\langle fm|\rho|fm\rangle = e^{\beta m}/Z$. Here $\beta = \ln(1+P) - \ln(1-P)$ is the spin-temperature parameter, and $P = \tanh(\beta/2) = 2\langle S_z\rangle$ is the electron spin polarization. The spin partition function is $Z = \Sigma_{fm} e^{\beta m}$. We expect the spin-temperature distribution to prevail when the spin exchange collision rate Γ_{se} between pairs of alkali-metal atoms is larger than any other relaxation rate of the system, which was the case for our experiments, as we discuss in more detail below.

Although the results of Fig. 3 were unexpected to us, they can be understood quantitatively by noting that the density operator ρ for an optically pumped alkali metal obeys the evolution equation

$$\dot{\rho} = \frac{1}{i\hbar}[H,\rho] + \sum_x \dot{\rho}_x, \tag{4}$$

where $H=A_g\mathbf{I}\cdot\mathbf{S}+(g_S\mu_B S_z-\mu_I I_z/I)B_z$ is the ground-state Hamiltonian for an alkali-metal atom in a magnetic field. The magnetic dipole coupling coefficient is A_g, the nuclear spin operator is $\mathbf{I}$, the g value of the electron is very nearly $g_S=2.0023$, the Bohr magneton is μ_B, and the magnetic dipole moment of the nucleus is $\mu_I=1.579\mu_N$, where μ_N is the nuclear magneton. The contribution to the evolution from the spin relaxation mechanism x is denoted by $\dot{\rho}_x$, where the most important mechanisms are the following.

Optical pumping: the evolution $\dot{\rho}_{\mathrm{op}}$ due to optical pumping. This evolution mechanism is proportional to the optical pumping rate Γ_{op} of Eq. (1). Without optical pumping, the steady-state density matrix will be given by the Boltzmann distribution $\langle fm|\rho|fm\rangle = e^{-E_{fm}/kT}/Z(T)$, where E_{fm} is the energy of the sublevel $|fm\rangle$, T is the absolute temperature of the gas, k is Boltzmann's constant, and the Boltzmann partition function is $Z(T)=\Sigma_{fm}e^{-E_{fm}/kT}$. The optical pumping efficiency also depends on how much of the polarization of the excited-state atoms returns to the ground state by spontaneous decay and quenching collisions with nitrogen molecules. These excited-state processes are included in our computer calculations.

Spin-exchange collisions: the evolution $\dot{\rho}_{\mathrm{se}}$ due to spin-exchange collisions between pairs of alkali-metal atoms at the rate Γ_{se} [5,6]. Spin-exchange collisions conserve the total angular momentum of the vapor and drive the density matrix toward the spin-temperature distribution mentioned above. Γ_{se} is proportional to the number density of alkali-metal atoms and therefore increases with temperature.

Spin-rotation collisions: the evolution $\dot{\rho}_{\mathrm{sr}}$ due to the spin-rotation interaction $\gamma\mathbf{N}\cdot\mathbf{S}$ between alkali-metal atoms and buffer-gas atoms or molecules [7,8]. This interaction couples the electron spin $\mathbf{S}$ to the rotational angular momentum $\mathbf{N}$ of the colliding pair and transfers spin to the translational angular momentum of the gas. The effects of the spin-rotation interaction can be parametrized by the isotope-independent rate Γ_{sr} (denoted by Γ_{SD} in [8]).

Hyperfine-shift collisions: the evolution $\dot{\rho}_{\mathrm{hs}}$ due to the hyperfine shift interaction $\delta A\mathbf{I}\cdot\mathbf{S}$ that occurs during collisions between an alkali-metal atom and a buffer-gas atom or molecule [8–10]. This rate can be parametrized by the isotope-independent Carver rate Γ_C. At relatively low magnetic fields of our experiments the hyperfine-shift collisions contribute mostly to the widths of the microwave resonance lines [10]. Both Γ_{sr} and Γ_C are proportional to the number density of the buffer gas, and Γ_{sr} often depends strongly on the gas temperature.

Diffusion to the walls: the evolution $\dot{\rho}_d$ due to the diffusion of the atoms to the cell walls, where most of the spin polarization is lost. The effects of diffusion are often modeled approximately with a uniform damping rate $\Gamma_d=D/l^2$, where D is the diffusion coefficient and l is a characteristic length, typically half the smallest dimension of the volume of pumped atoms in the cell. For the experimental results shown in Fig. 3, we estimate that the spin-exchange rate was $\Gamma_{\mathrm{se}}=4.6\times10^4\ \mathrm{s}^{-1}$. The other important spin relaxation rates are the spin-rotation rate $\Gamma_{\mathrm{sr}}=521\ \mathrm{s}^{-1}$, the Carver rate $\Gamma_C=107\ \mathrm{s}^{-1}$, the diffusion rate $\Gamma_d=47\ \mathrm{s}^{-1}$, and the optical pumping rate $\Gamma_{\mathrm{op}}=500\ \mathrm{s}^{-1}$.

As we will show below, one can obtain steady-state solutions to the evolution equation Eq. (4) with $\dot{\rho}=0$ with computers, and the results are in very good agreement with our observations. But one can understand the reason for the curious signal reversals without elaborate computer calculations by considering the spin-temperature limit, when Γ_{se} is much larger than any other characteristic rate of the system. Our experimental conditions for weak pumping light are actually quite close to this limit. In the spin-temperature limit, the sublevel populations are determined by a single parameter, which we will take to be the polarization $P=\tanh(\beta/2)$. Under these conditions, $\langle A\rangle$ will be a well-defined function of P, and one can readily see that $\langle A\rangle\to1$ when $P\to0$ and all atomic sublevels are equally populated, and $\langle A\rangle\to0$ when $P\to1$ and all atoms are in the nonabsorbing sublevel $|44\rangle$. How $\langle A\rangle$ changes from 1 to 0 with increasing P for various laser tunings can be understood with reference to Fig. 4. Figures 4(a) and 4(b) show the two laser frequencies, the specific absorptions $\langle fm|A|fm\rangle$ (narrower bars), and the sublevel occupation probabilities $\langle fm|\rho|fm\rangle$ (wider bars), for each ground-state sublevel. A spin-temperature distribution is assumed. In Fig. 4(a), the laser is tuned to excite atoms predominantly from the upper hyperfine multiplet with $f=4$. As the laser intensity increases, $\langle A\rangle=\Sigma_{fm}\langle fm|A|fm\rangle\langle fm|\rho|fm\rangle$ decreases, because the populations of weakly absorbing sublevels increase with increasing laser intensity and increasing polarization. Figure 4(b) shows the case where the laser is tuned to excite atoms predominantly from the lower multiplet with $f=3$. If the pumping intensity is not too great, the specific absorption $\langle A\rangle$ will increase with increasing intensity, because the populations of strongly absorbing sublevels grow with the increasing polarization produced by the pumping laser. We already mentioned that, irrespective of the laser detuning, sufficiently fast pumping with circularly polarized $D1$ light will cause the specific absorption to vanish, $\langle A\rangle\to0$, because all atoms will be pumped to the nonabsorbing "end state" $|44\rangle$. So, if the laser is tuned to cause maximum depopulation of atoms from the sublevels with $f=3$, the specific absorption will at first increase with increasing laser intensity $\mathcal{S}$ and increasing polarization P, and will then decrease to zero.

In Fig. 4(c) we show the result of finding the steady-state solutions of (4) with a computer program that takes the most important relaxation processes mentioned above into account. We also account for the spatial variation of the pumping rate due to attenuation of the laser beam in the vapor. For the laser detuning that pumps atoms predominantly from sublevels with $f=4$, the specific absorption $\langle A\rangle$ decreases monotonically with increasing optical pumping rate. For the laser frequency that pumps predominantly from sublevels with $f=3$, $\langle A\rangle$ first increases with the pumping rate and then decreases. The calculation (lines) agrees well with the experimental data (solid circles in the figure). Figure 4(d) shows the $\langle A\rangle$-P curves for the two laser detunings. Here P is

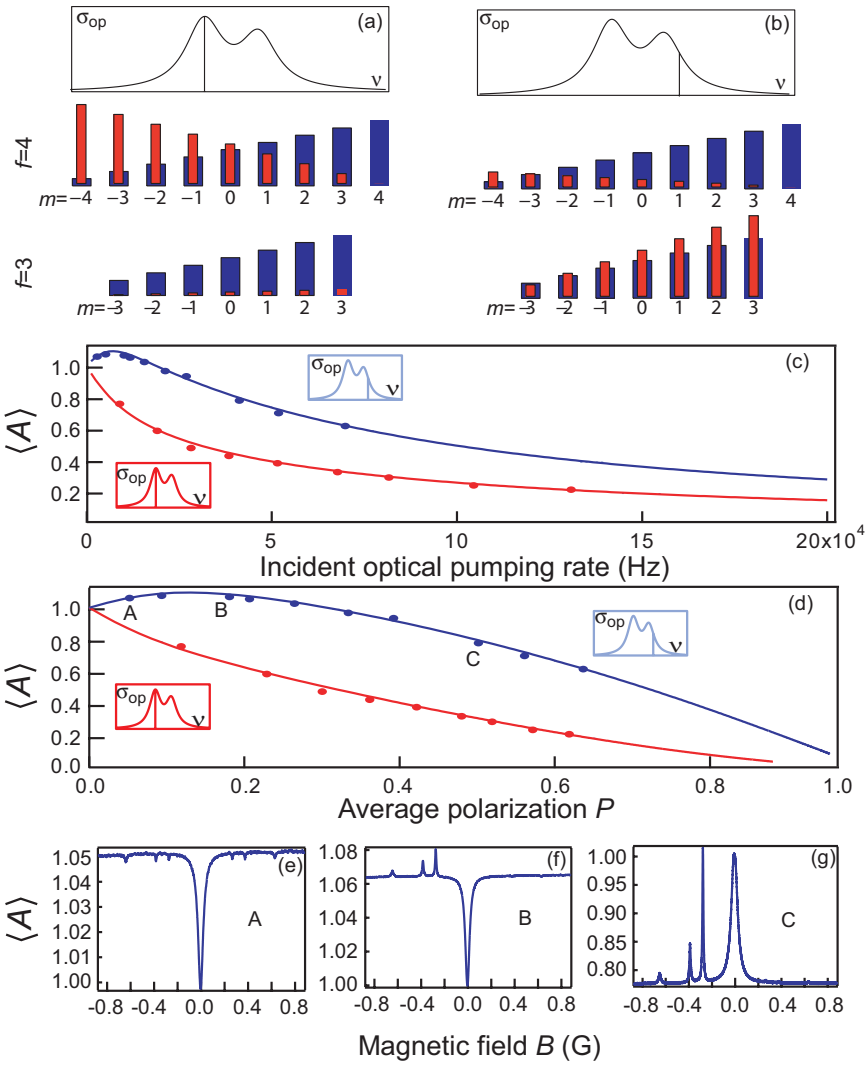

FIG. 4. (Color online) (a), (b) $\langle fm|A|fm\rangle$ (narrower bar) and $\langle fm|\rho|fm\rangle$ (wider bar) for each ground-state sublevel at the two different laser detunings. (c) Specific absorption $\langle A\rangle$ versus optical pumping rate curves. (d) Specific absorption $\langle A\rangle$ versus average polarization P curves. The upper trace is for the laser frequency 335 122.0 GHz, and the lower trace is for the laser frequency 335 109.0 GHz. Lines are calculations and solid circles are experimental data. (e), (f), (g) $\langle A\rangle$-B curves corresponding to points A, B, and C in (d), respectively.

the average polarization, which is calculated using $P=\Gamma_{op}/(\Gamma_{op}+\Gamma_{sd}+\epsilon\Gamma_d)$ and averaged along the beam path in the vapor (along which Γ_{op} decreases). Here, ϵ is defined as $1+\epsilon=\langle F_z\rangle/\langle S_z\rangle$ [11]. The microwave resonance transitions with $\Delta m=\pm 1$ always remove spin from the vapor and cause P to decrease. If the laser is tuned to excite atoms predominantly from the sublevels with $f=4$, when $\langle A\rangle$ decreases monotonically from 1 to zero with increasing P, we expect the microwave resonances to always increase the specific absorption for any laser power. The situation is more interesting when the laser is tuned to excite atoms predominantly from the sublevels with $f=3$. Then if the laser intensity is small enough that $d\langle A\rangle/dP>0$, the microwave resonances actually decrease the specific absorption and the vapor becomes more transparent. But if the laser is intense enough that $d\langle A\rangle/dP<0$, small microwave resonances correspond to an increase in the specific absorption.

Three points (A, B, and C) from the upper trace in Fig. 4(d) are chosen to show the experimental results. The dependence of specific absorption $\langle A\rangle$ on the magnetic field B is shown in Figs. 4(e)–4(g). Point A is in the range where $d\langle A\rangle/dP>0$ and $\langle A\rangle>1$. So both the magnetic resonances and the zero dip show as absorption dips, as in Fig. 4(e). Moreover, since the atoms are weakly polarized and close to the spin-temperature limit, the population difference between the initial and final states of the resonant transition was about the same for positive and negative azimuthal quantum numbers, and magnetic resonances appeared on both sides of the zero dip. Point B is in the range where $d\langle A\rangle/dP<0$ and $\langle A\rangle>1$. Since the microwave field causes only a small change in polarization, but the residual transverse field is big enough to completely destroy the spin polarization, magnetic resonances appear as positive absorption peaks and the zero dip appear as negative peaks, as is shown in Fig. 4(f). Point C is in the range where $d\langle A\rangle/dP<0$ and $\langle A\rangle<1$, so both the zero dip and magnetic resonances appear as absorption peaks, as in Fig. 4(g). Because most of the atoms were in states with positive m for the more intense pumping light of situations B and C, we could barely observe magnetic resonances on the other side of the zero dip, since these corresponded to atoms with negative m.

Considering a more general case, the spin-temperature distribution does not always exist, we need to use detailed density-matrix modeling to calculate the resonance signals. For illustration, we tested a cell with a different buffer-gas mixture (50 torr N_2 and 480 torr Ar). The incident laser power density $\mathcal{S}$ was about 0.1 mW cm^{-2} for all the laser

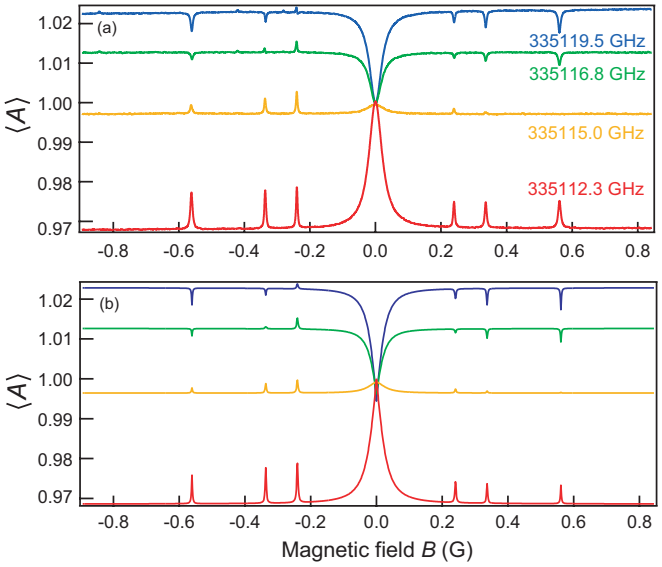

FIG. 5. (Color online) Experimental results and simulations for a different cell with buffer-gas mixture of 50 torr N_2 and 480 torr Ar. (a) Measured $\langle A \rangle$ versus magnetic field B curves at four different laser frequencies. (b) Simulation results.

detunings. The distance between the front and rear walls of the cell was 1.7 cm. The temperature was 90 °C. This lower temperature reduces the number density of Cs atoms and leads to a much smaller spin-exchange rate. In spite of this, reversals of the magnetic resonance signals were also seen in this cell. Figure 5 shows the comparison between the experimental data of Fig. 5(a) and the computer simulations of Fig. 5(b) for four different laser frequencies. The simulated results were calculated with the detailed model mentioned above. The values of the modeling parameters were the optical pumping rate $\Gamma_{op}=20\ s^{-1}$, the spin-exchange rate $\Gamma_{se}=4500\ s^{-1}$, the spin-rotation rate $\Gamma_{sr}=919\ s^{-1}$, the Carver rate $\Gamma_C=107\ s^{-1}$, and the diffusion rate $\Gamma_d=28\ s^{-1}$. The simulation is strikingly similar to the experimental data.

In summary, we have experimentally demonstrated an unusual signal reversal phenomena of the magnetic resonances of ground-state alkali-metal atoms pumped by $D1$ circularly polarized laser light. Under this circumstance, the hyperfine splitting has to be at least partially optically resolved, and the optical frequency of the pumping light should be tuned to reach near the lower hyperfine multiplets. The phenomenon cannot be explained by the conventional two- or three-level modelings, or even a multilevel modeling with a universal damping rate. A valid theoretical explanation involves a density-matrix modeling with two important spin-relaxation mechanisms, spin-rotation interaction and spin-exchange interaction. The reversal phenomena are more pronounced especially when a rapid spin-exchange rate produces a spin-temperature distribution. These phenomena came to our attention in connection with work on the Defense Advanced Research Projects Agency chip scale atomic clock program, where it is hoped that small, laser-pumped Cs or Rb vapor cells, similar to the ones of this experiment, could form the basis of a useful new type of atomic clock. The relatively high densities of alkali-metal vapors, which causes a high spin-exchange rate, and the narrow-line diode lasers used to pump the miniature cells of CSAC clocks often lead to conditions similar to those reported here. For microwave-interrogation atomic clocks, some care should be exercised not to operate these systems with parameters close to those that reduce or reverse the resonance signals.

This work was supported by the Air Force Office of Scientific Research, with supplemental support from the Defense Advanced Projects Agency.

[1] W. Happer, Rev. Mod. Phys. **44**, 169 (1972).
[2] J. Fricke, J. Haas, E. Lüshcer, and F. A. Franz, Phys. Rev. **163**, 45 (1967).
[3] B. S. Mathur, H. Tang, and W. Happer, Phys. Rev. A **2**, 648 (1970).
[4] L. W. Anderson and A. T. Ramsey, Phys. Rev. **124**, 1862 (1961).
[5] L. C. Balling, F. M. Pipkin, and R. J. Hanson, Phys. Rev. **133**, A607 (1964).
[6] F. Grossetête, J. Phys. (Paris) **25**, 383 (1964).
[7] R. A. Bernheim, J. Chem. Phys. **36**, 135 (1962).
[8] D. K. Walter, W. M. Griffith, and W. Happer, Phys. Rev. Lett. **88**, 093004 (2002).
[9] J. Vanier and C. Audoin, *The Quantum Physics of Atomic Frequency Standards* (A. Hilger, Philadelphia, 1989).
[10] P. J. Oreto, Y.-Y. Jau, A. B. Post, N. N. Kuzma, and W. Happer, Phys. Rev. A **69**, 042716 (2004).
[11] S. Appelt, A. B. Baranga, C. J. Erickson, M. Romalis, A. R. Young, and W. Happer, Phys. Rev. A **58**, 1412 (1998).